Sensitivity of modeled estuarine circulation to spatial and temporal resolution of input meteorological forcing of a cold frontal passage

Robert J. Weaver*†, Peyman Taeb†, Steven Lazarus†, Michael Splitt†, Bryan Holman†, Jeffrey Colvin†

†Department of Marine and Environmental Systems
150 W. University Blvd.
Florida Institute of Technology
Melbourne, FL 32901, U.S.A.

*Corresponding Author:
Robert J. Weaver
Ph: 321-674-7273
Email: rjweaver@fit.edu

LRH: Weaver, *et al.*
RRH: Estuarine circulation input resolution sensitivity

Abstract

In this study, a four member ensemble of meteorological forcing is generated using the Weather Research and Forecasting (WRF) model in order to simulate a frontal passage event that impacted the Indian River Lagoon (IRL) during March, 2015. The WRF model is run to provide high and low, spatial ($0.005°$ and $0.1°$) and temporal (30 min and 6 h) input wind and pressure fields. The four member ensemble is used to force the Advanced Circulation model (ADCIRC) coupled with Simulating Waves Nearshore (SWAN) and compute the hydrodynamic and wave response. Results indicate that increasing the spatial resolution of the meteorological forcing has a greater impact on the results than increasing the temporal resolution in coastal systems like the IRL where the length scales are smaller than the resolution of the operational meteorological model being used to generate the forecast. Changes in predicted water elevations are due in part to the upwind and downwind behavior of the input wind forcing. The significant wave height is more sensitive to the meteorological forcing, exhibited by greater ensemble spread throughout the simulation. It is important that the land mask, seen by the meteorological model, is representative of the geography of the coastal estuary as resolved by the hydrodynamic model. As long as the temporal resolution of the wind field captures the bulk characteristics of the frontal passage, computational resources should be focused so as to ensure that the meteorological model resolves the spatial complexities, such as the land-water interface, that drive the land use responsible for dynamic downscaling of the winds.

ADDITIONAL INDEX WORDS: *Coastal Lagoon, Estuarine Dynamics, Meteorological Forcing, Hydrodynamics, Wind-Driven Current, Wind Set-Up, Numerical Modeling, ADCIRC, WRF.*

Introduction

Past studies focusing on surge, flooding and inundation have demonstrated the importance of the wind field, especially those involving high intensity events such as tropical cyclones. While resolving the coastal ocean, the hydrodynamic simulations were generally not extended into lagoons and estuaries and the model response within these regions and associated bays and tributaries is not well understood. There are two primary issues that continue to hinder progress, namely how to improve the wind field in these areas, and hydrodynamic model resolution – both of which carry a computational expense. Both extratropical cyclones and strong frontal passages, which impact Central Florida during the winter months, are often accompanied by rapid changes in wind speed and direction and thus can have a pronounced impact within an estuarine system. Capturing these events may require both high spatial and temporal resolution in the meteorological forcing.

Strong frontal passages occur frequently in Central Florida, peaking at about 8 fronts per month, and can have a pronounced impact within an estuarine system (DiMego et al., 1976). Due to the relatively small spatial scales associated with coastal estuarine environments and the generally large spatial meshing

used by the current suite of operational meteorological models, the wind fields used to drive estuarine circulation are typically under resolved in space. When predicting the response of a water body to meteorological forcing, experts agree that "it's the wind" and errors in the modeled wind drive the hydrodynamic forecast error. Forecast errors can be compounded when the area of interest is a coastal estuary with length scales less than or on the order of the available resolution of the operational meteorological models.

One consequence is that the meteorological model will under (over) predict the wind forcing due to the application of a land (water) mask to the winds over areas where the circulation model sees water (land). In addition, abrupt temporal changes in wind direction and magnitude may be lost when simulating a fast moving frontal system if the temporal resolution is insufficient in relation to the speed of the front. Given the limited computational resources available for ensemble simulations, and availability of limited "off-the-shelf" wind products, this study examines the sensitivity of the Indian River Lagoon Estuary System to the spatial and temporal resolution of the meteorological forcing that coincides with a frontal passage during March, 2015.

Background

The Indian River Lagoon (IRL) is a shallow and narrow restricted estuarine system (Kjerfve, 1986), approximately 195 km in length, 2-4 km in width, and 1-3 m in depth (Smith, 1990). In a typical estuarine system, freshwater discharge, tidal action, and atmospheric forcing are the three primary factors that influence water movement (Reynolds-Fleming *et al.*, 2004). Tidal forcing is reduced due to the morphology, orientation, and connection of the system to the ocean (Luettich *et al.*, 2002). As a result of the restricted nature of the northern IRL, the movement of water throughout most of the lagoon is driven primarily by meteorological processes (Smith, 1990). The geometry for this estuary is also unique since it is long and narrow with many cuspate features creating partially sheltered bays. There are natural tributaries that flow into the IRL, and man-made canals that are part of a statewide surface water plumbing system designed to release excess freshwater to tide. Additionally, the dredging of the Intracoastal Waterway resulted in the creation of a string of spoil islands, and residential development produced a network of canals.

When studying circulation in shallow lagoon systems such as the IRL, it has become commonplace to estimate flow patterns and simulate this circulation using computational fluid dynamics (CFD) (Cheng, Casulli, and Gartner, 1993; Reynolds-Fleming *et al.*, 2004; Luettich *et al.*, 2002). The CFD provides a

synoptic description of the circulation for the basin which, until recently, has had very few *in-situ* measurement stations. Recent modeling results have indicated that large scale changes of surface elevation (set-up) due to periodic and event scale atmospheric disturbances drive the circulation in those portions of the IRL isolated from the ocean by the proximity of the inlets (Weaver *et al.*, 2016). Studies conclude that a surface oscillation with a near semi-diurnal or near diurnal period can correspond to strong wind events that occur in small lagoon systems such as the IRL (Vilibric *et al.*, 1990, Luettich *et al.*, 2002, Weaver *et al.*, 2016).

Recognizing the wind dominated nature of the IRL (and other estuary systems), this study aims to investigate the sensitivity of localized circulation to the spatial and temporal resolution of wind driven forcing. For a prediction of circulation to be accurate, the winds must be represented at a scale that captures the continually forced response of the natural system. Unfortunately, while the suite of National Center for Environmental Prediction (NCEP) models are run at relatively high resolution time-steps (i.e., on the order of 10 minutes, http://www.emc.ncep.noaa.gov/GFS/doc.php#timintsch), operational meteorological model output is generally available at time intervals ranging from 1 to 6 h. For example, the NCEP Global Forecast System (GFS) model and North American Mesoscale Forecast System (NAM, Janjić *et al.* 2005) model are available at a 3 h time resolution[1], and the ensemble implementation of the GFS (the Global Ensemble Forecast System, GEFS; EMC, 2003) has output at 6 h resolution. Archived meteorological analysis data sets, for retrospective studies, from these operational models or from models such as the Climate Forecast System (CFS) Version 2 (CFSv2, Saha *et al.* 2014) are often only available at 6 h resolution. Such temporal resolutions may not be adequate to capture the finer details of a fast moving cold front as it passes over a narrow lagoon.

The spatial resolution of the meteorological forcing is also important for narrow coastal lagoon systems. For example, the GFS is available at resolutions of 2.5, 1.0, 0.5, and 0.25 degrees with a 100 fold increase in the size of the 2-D fields between the extremes. Even at the higher end of operational model resolution, the 12 km NAM cannot resolve the highly nuanced land – water mask for many of these systems. Furthermore, high resolution products such as the 2.5 km Real-Time Mesoscale Analysis (RTMA, De Pondeca *et al.* 2011) are also problematic, in part because they typically draw from scales that are larger than the grid spacing implies. As a result, a long narrow estuary such as the IRL will invariably be forced with a wind field that is based on roughness lengths that do not adequately resolve the land – water physics (Cheng and Byun, 2008). As an alternative, users can run their own simulations

[1] NAM output is now available at 1 h intervals through forecast hour 36.

such as the Weather Research and Forecast (WRF) model (Skamarock *et al.*, 2008). In this capacity, one can then control the spatial and temporal resolution of the model output – with the obvious caveat that the particular choices will impact computational time.

The WRF model has been used to downscale lower resolution GCM model output in climate studies. For example, Mallard *et al.* (2014) focused on the challenges of properly representing lake temperatures by using the WRF model to downscale output from the Community Earth System model (CESM) to a resolution sufficient to resolve lakes. Operational meteorological model output from the GFS was used (in hindcast mode) to force WRF simulations in order to assess wave energy in Hawaii (Stopa *et al*., 2011). The higher resolution WRF simulations were crucial for defining the wave field to the lee of Maui and Hawaii Island. Muller *et al.* (2007), in a study on providing atmospheric forcing to a regional oceanic model, noted that higher resolution in the WRF was paramount for resolving coastal small-scale features. Santos-Alamillos *et al.* (2015) used an updated very high resolution (100 m) land use data set to test the impact of an improved representation of surface elements on the WRF wind field. Their results indicated a reduction in the wind speed bias with minimal impact on wind direction. In simulations where the spatial and temporal scales of the meteorological wind forcing on wave fields in a semi-enclosed basin (northwest Mediterranean) were varied, Alomar (2012) improved the timing of wave peaks for storm events by increasing the spatial resolution of the wind input (from 12km to 4km). Conversely, hindcasts of maximum wave height were improved by increasing the temporal resolution (from 6 h to 3 h). In the present study, both temporal and spatial resolutions are examined for a frontal system that passed over the IRL during March of 2015.

Table 1: Matrix of WRF simulation resolutions

Model Scenarios	Low Spatial Resolution (LS) $0.1°$	High Spatial Resolution (HS) $0.005°$
Low Temporal Resolution (LT) 6 h	Low:Low (LT-LS)	Low:High (LT-HS)
High Temporal Resolution (HT) 30 min	High:Low (HT-LS)	High:High (HT-HS)

Methodology

Meteorological forcing (wind and pressure) is generated for the 3-day period of 5-8 March, 2015. The forcing, shown in Table 1, consists of 4 scenarios constructed via the pairing of a high (low) spatial (HS (LS)) resolution wind field at 0.005 (0.1) degrees, Figures 1(a) and (b), with a high (low) time (HT (LT)) resolution wind field at 30 min (6 h).

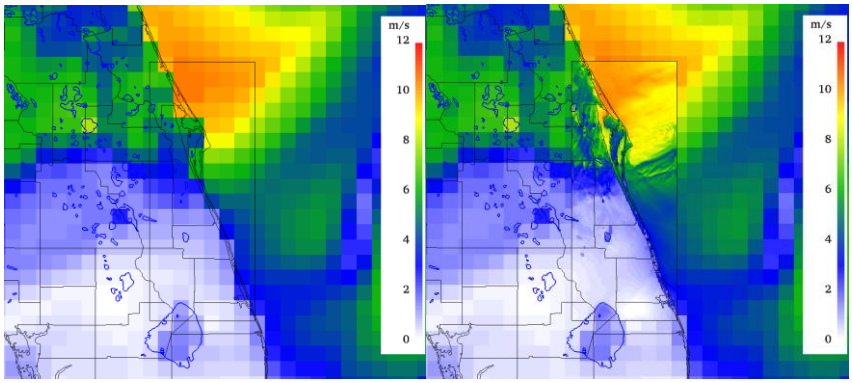

(a) (b)

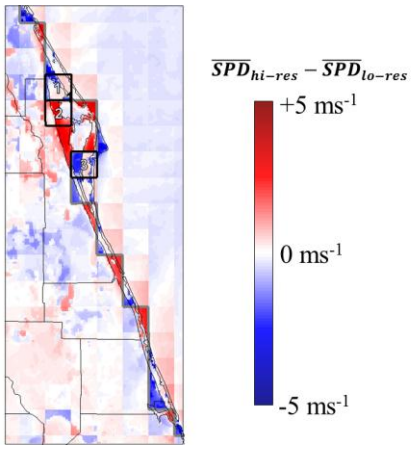

(c)

Figure 1: Sample WRF model wind speed on the native grid for the (a) LS, $0.1°$, resolution, and the (b) nested HS, $0.005°$, resolution meteorological simulations. (c) Wind speed difference (ms^{-1}) averaged over the entire simulation (HS - LS resolution) with the inset boxes highlighting the model validation and analysis locations (shown in more detail in Fig. 3). The land - water mask is delineated on the HS resolution inner grid in panel (b) with higher winds over water and lower winds over land. The contours in (c) highlight the course handling of the land-sea interface by the LS resolution model.

Meteorology: Model Configuration

The meteorological simulations were performed using the WRF model V3.4.1 with a triple (one-way) nested configuration consisting of a parent domain of 13.5 km resolution (LO_RES) and an inner (highest resolution) nest of 0.5 km resolution (HI_RES), Figure 1(b). The simulations were performed using the Yonsei University scheme boundary layer parameterization (non-local closure, Hong *et al.*, 2006) along with the MM5 Monin–Obukhov surface layer physics scheme (Jimenez *et al*., 2012). The National Centers for Environmental Prediction (NCEP) Global Forecast System (GFS) 0.5° resolution operational analyses (3-hourly intervals) are used for initial conditions and boundary conditions for the simulations. The NCEP-GFS was selected based on its ability to generate the estimated wind speed distributions and wind energy fluxes closest to the ones obtained with measured wind data (Carvalho *et al.*, 2014). In order to ensure that the forcing obtained from the meteorological simulations did not drift significantly from the observed timing of the frontal passage, a series of 12 overlapping short-term WRF forecasts (9 h) were stitched together to produce a continuous forcing field for the hydrodynamic model. A model spin-up period of 3 h was disregarded for all but the first model simulation. The model output was converted from a native Lambert Conic Conformal projection to a regular latitude/longitude (lat/lon) coordinate system for input into the hydrodynamic model. Here, the WRF 13.5 km outer domain was used to create the LS resolution forcing (0.1° by 0.1° lat/lon grid, a resolution appropriate for modeling oceanic mesoscale eddies), while the 500 m inner nest was interpolated to create the HS resolution forcing (0.005° by 0.005° lat/lon grid, a resolution that captures the estuary land/water mask but does not require atmospheric large eddy simulations). The two sets of temporal resolution are generated by selecting WRF output every 30 min to create the HT resolution forcing and sampling that data every 6 h (common available operational meteorological model output interval as described above) for the LT forcing.

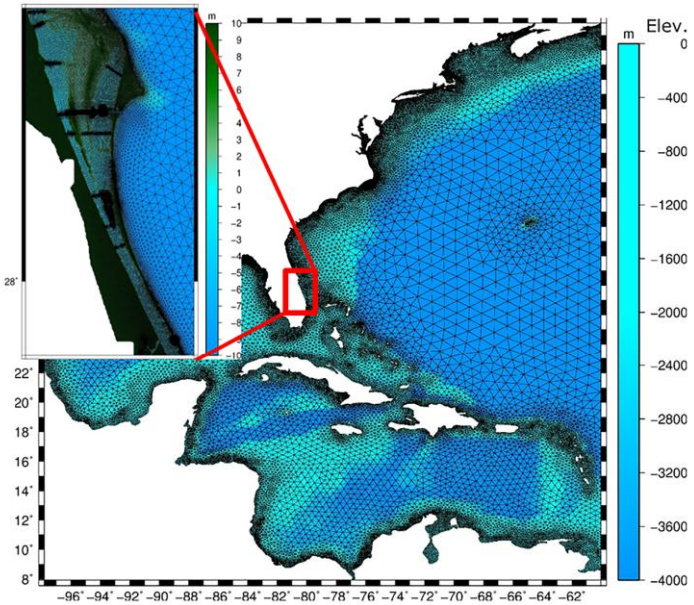

Figure 2: ADCIRC +SWAN model domain encompassing the North West Atlantic, with zoomed inset over the northern IRL. Note the high resolution around the channels and causeways. The mesh consists of 167652 nodes with a minimum resolution in the IRL of 25 m.

Hydrodynamics: Models and Domain Configuration

The ADvanced CIRCulation (ADCIRC) model system (Luettich and Westerink, 2004; 2006) is adapted to the IRL and configured to run in 2-dimensional depth-integrated mode (2DDI). Forced with tidal constituents, wind and pressure fields, ADCIRC 2DDI produces a prediction of surface elevation and 2-D depth averaged water current velocities. To compute predictions of the wave field, Simulating Waves Nearshore (SWAN), a phase averaged wave model, is dynamically coupled with ADCIRC 2DDI (ADCIRC+SWAN) (Dietrich *et al.*, 2012; Dietrich *et al.*, 2011; Hope *et al.*, 2013). The elevations and currents computed in ADCIRC are passed to SWAN which computes the wind waves and then returns wave characteristics to ADCIRC to compute the circulation. The water levels, current velocities and phased averaged significant wave heights are output from the ADCIRC+SWAN model. For this study we use a spatially varying depth dependent bottom friction coefficient (in water) based on a Manning's n type formula, with $n = 0.02$ while the surface roughness for flow over inundated land is determined from the National Land Cover Dataset (NLCD) (Arcement and Schneider, 1989; Fry, *et al.*, 2011; Luettich and Westerink, 2006). A minimum value for the drag coefficient is set, $C_{D_{min}} = 2.0 * 10^{-3}$.

The ADCIRC+SWAN model configuration is the same for all simulations. The model domain is a 167652 node unstructured mesh, with grid resolution varying from a minimum on the order of 25 m in the inlets, canals and channels of the IRL, to over 10 km in the Atlantic Ocean, Figure 2. For each of the simulations, the fields are interpolated from the input meteorological grid to each node in the ADCIRC model domain without any adjustments. The focus of the analysis presented here is the central IRL, shown in the inset to Figure 2. The topography for the domain is interpolated from a 5ft horizontal resolution Digital Elevation Model (DEM) created for Brevard County based on 2007 LIDAR data. The bathymetric data is

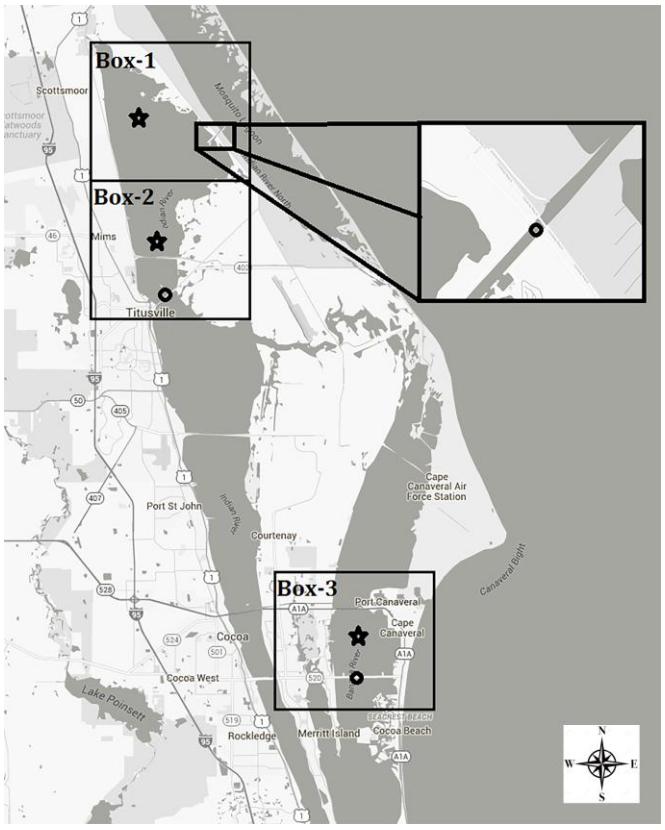

Figure 3: The north-central IRL analysis region, water regions are shaded gray. Circulation model validation points are indicated by the open circles and the open stars indicate the location of the inter-model comparison points.

adjusted based on NOAA nautical charts to include a representation of the Intracoastal Waterway (ICW), a 3,000 mile long intermittent inland waterway along the East and Gulf Coasts of the United States of America. Model topography is referenced to vertical datum NAVD88.

Model Validation

The coupled model system is validated for surface elevation against station data time series for water level corresponding to the passage of the March, 2015 frontal system. The validation of the response of the circulation model will provide confidence in the models ability to accurately predict the response of the sea surface to the variations in the input meteorological forcing. The HS and LS resolution wind forcing are validated against the Parrish Park WeatherFlow station located northeast of Titusville, Florida on the Indian River.

The ADCIRC model is forced by wind and tides for the validation simulation. The tides are modeled for 124 days prior to the March event to ensure adequate time for the propagation of the tidal signal into the shallow estuary. The wind forcing is added one week prior to the March event in order to develop the wind driven circulation that dominates IRL. Model output from each of the spatial and temporal ensemble members is plotted against station data over the time period, 00Z 5 March 00:00 2015 through 00Z 8 March 00:00 2015. Each model simulation is validated against surface elevation stations in each of the three WRF grid boxes shown in Figure 3 by the open circles (water locations are shaded gray). The validation sites are limited to the location of *in-situ* measurement stations that were collecting data during the March event. The grid box size (13.5 km) matches that of the low spatial resolution WRF outer nest. Box 1 and Box 2 are located in Northern Indian River, and Box 3 is located in the central Banana River. The validation point for Box 1 is a USGS station in the Haulover Canal, separating the Mosquito Lagoon from the Northern IRL (Figure 3, inset). The Lagoon (over water) portion of Box 1 is resolved as water by both the HS and LS resolution WRF. In Box 2 the validation point is located on the A. Max Brewer fishing pier in Titusville, FL, near the southern edge of the box. Box 2 is treated as land by the low spatial model while both the land and water is resolved by the high spatial resolution model with water at the Box 2 validation point. The validation point in Box 3 is a station

Table 2: Land-use agreement between High and Low spatial resolution suite members of the analyses Boxes.

Spatial Resolution	Box 1	Box 2	Box 3
Low (LS)	Water	Land	Water
High (HS)	81% Water / 19% Land	40% Water / 60% Land	54% Water / 46% Land

located on the FL 520 Causeway. The area of Banana River which is covered in Box 3 is treated as water by the low spatial meteorological forcing, land regions in this box are not resolved by LS resolution forcing, Table 2. The validation point in Box 3 is treated as water in both cases; however, the land effects are not resolved in the low resolution case.

Time Series Analysis

Once validated, we examine the sensitivity of the wave heights and sea surface elevation to the temporal and spatial resolution of the wind forcing. Analysis of the differences between the low and high, spatial and temporal resolution solutions is performed at points that are located more centrally in the lagoon portion of each boxed domain, as indicated by the stars in Figure 3.

Time series of water elevation and significant wave height, H_S, from each of the four ensemble members is examined. Water level and wave height differences between the four members are also evaluated. Wind forcing and water elevation, as well as the wind forcing and H_S, are analyzed using the cross-autocorrelation method in which a correlation is calculated between time series of surface elevations, significant wave heights and shifted (time lagged) wind magnitude. Coefficients of determination are calculated (Wackerly *et al.*, 2007).

Table 3: Modeled versus observed water elevation RMSE (m) for each of the 4 case scenarios found in Table 1.

Resolution	RSME (m)		
Temporal Spatial	**Haulover Canal**	**A. Max Brewer Memorial Causeway**	**W. Cocoa Beach Causeway**
HT-HS	0.001	0.158	0.033
HT-LS	0.268	0.364	0.143
LT-HS	0.037	0.171	0.015
LT-LS	0.270	0.378	0.128

Results

The ability of the HS resolution WRF runs to better represent the wind field over the IRL is exemplified in the comparison of the two model runs (HS versus LS resolution) to observed wind speeds provided by the Parrish Park WeatherFlow station over the Indian River just northeast of Titusville, Florida. The station provided 5 minute average wind speed with a 3-sec gust for the interval. The bias/root-mean-squared error (RMSE) for the wind speed was $-2.6\ \mathrm{ms}^{-1}$ / $+3.2\ \mathrm{ms}^{-1}$ for the LS resolution WRF and $+0.1\ \mathrm{ms}^{-1}/+1.8\ \mathrm{ms}^{-1}$ for the HS resolution WRF at this location. The maximum wind speed at this location provided by the LS/HS resolution run was $6.7\ \mathrm{ms}^{-1}/11.8\ \mathrm{ms}^{-1}$ while the observed maximum

was $13.2\ \mathrm{ms}^{-1}$. Note that the Parrish Park wind magnitude observations are at 18 feet (5.5 m) and would be somewhat higher at the modeled 10 m level. Given that the WRF winds tend to under predict

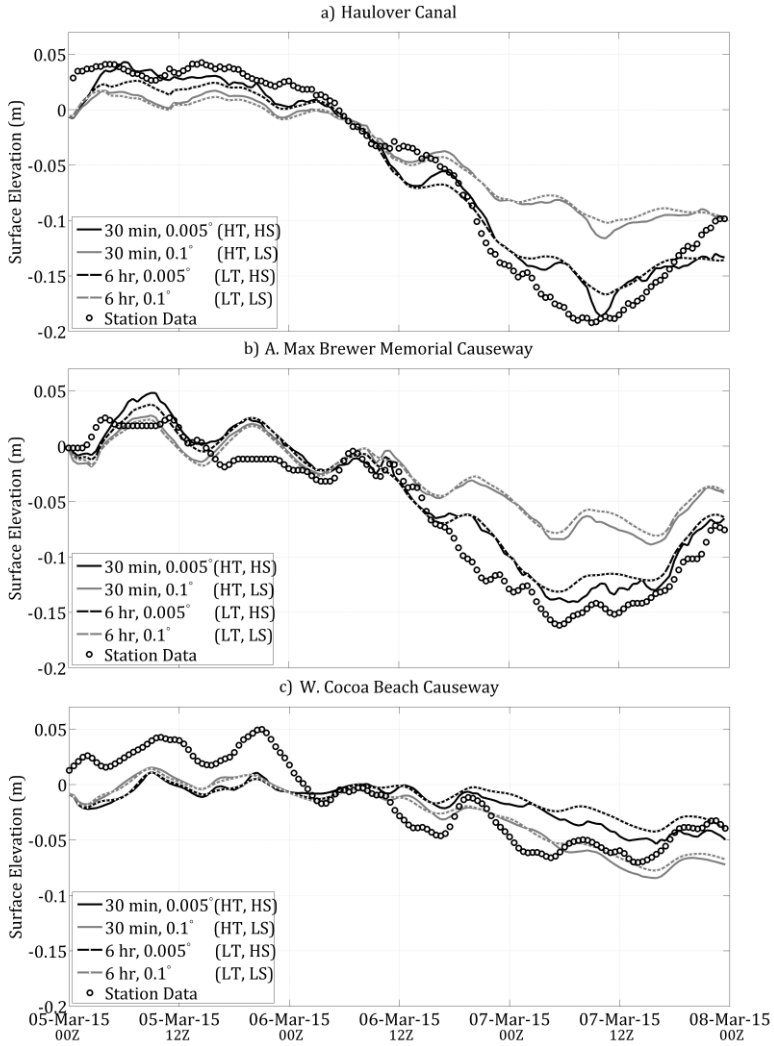

Figure 4: Model surface elevation (m) validated against station data, for the boxes shown in Fig. 4, for the three-day period 5-8 March 2015 (a) Box 1: Haulover canal; data from U. S. Geological Survey (USGS). (b) Box 2: A. Max Brewer Memorial Pkwy, data from St. Johns River water management district. (c) Box 3: West Cocoa Beach Causeway, data from St. Johns River water management district. Meteorological and tidal forcing are used in the validation model.

the station measurements, the modeled response to the WRF input wind filed is expected to under predict the water level station data.

Model Validation

The WRF forced ADCIRC+SWAN simulations are validated against observations. As indicated by the comparison of modeled wind speed to measured wind speed, at each validation station the model results under-predict the set-up and set-down. The RMSE for HT-HS and the LT-HS are the lowest of the four model scenarios. Increasing the spatial resolution reduces the RMSE more than increasing temporal resolution, Table 3.

At the Haulover canal in Box 1, the model data under predicts the peak elevation change in the canal, Figure 4(a). The model does capture the phasing of the elevation signal in the canal. In Box 2, a water level station is fixed to the A. Max Brewer Causeway, Figure 4(b). The RMSE is less than 0.18 m for both of the HS resolution simulations. In Box 3, at the Cocoa Beach Causeway, the model and station data are also in good agreement, with an RMSE less than 0.035 m for the HS resolution simulations, Point-3, Figure 4(c). Any differences in model and station

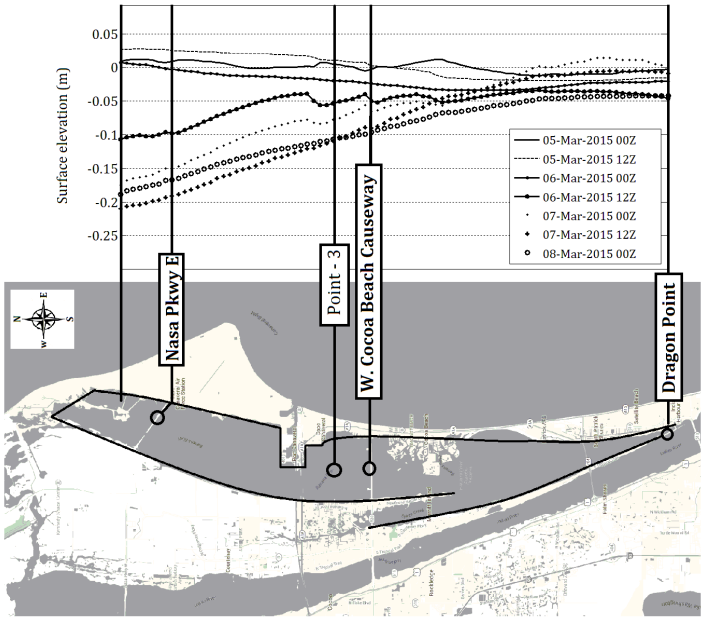

(a)

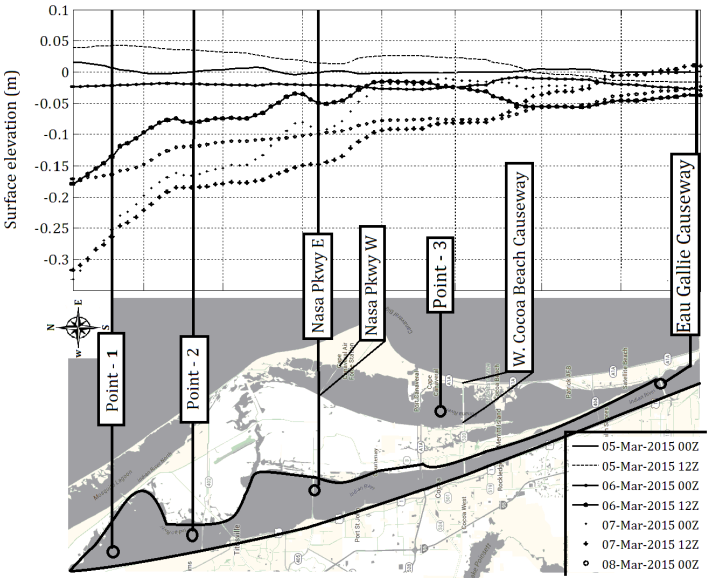

(b)

Figure 5: Temporal snapshots of the cross-sectional surface elevation (m) along the (a) Banana River, and (b) Indian River from the HT-HS simulation. Values shown (various lines) are 12 hours apart for the 72 h period beginning 00 Z 5 March 2015. Figure is oriented with North-South on the horizontal axis, water regions are shaded gray.

elevations at the first data point the 00 Z 5 March 2015 are based on the long spin up time (described above) and do not impact the differences in RMSE or analysis of the model comparison results.

At the Banana River location, Point-3, the water elevation experiences relatively small deviations from the model mean water level. The station is located near an inflection point in the Banana River, *i.e.*, a point about which the water levels pivot with relatively little local change in elevation. In the case of sustained northerly winds, the water elevation north of this point is set-down as water is pushed from the northern end of the basin southward. In this scenario, the water flows to a point of constriction south of the station at Dragon Point, Figure 5(a), creating localized set-up as the water is restricted from flowing into the IRL by a narrow conveyance. The surface elevation transects in Figures 5(a) and 5(b) extend from the northern Banana River to the outlet into the IRL at Dragon Point and from the northern IRL to the constriction at Wabasso Bridge. These transect time series aid in conceptualizing the time varying lagoon surface elevation during the event. Early in the simulation, when the wind is southerly,

Table 4: Differences between the spatial simulation results and differences between the temporal resolution results for both surface elevation and H_s at each point are provided in this table. The maximum spatial (temporal) difference is calculated by subtracting the LS from HS (LT from HT).

	Surface Elevation (cm)		H_s (cm)	
Points	Max Spatial Diff.	Max Temporal Diff.	Max Spatial Diff.	Max Temporal Diff.
Point -1	-11 HT	-4 HS	4 HT	2.6 HS
Point -2	-8 HT	3 HS	6 HT, LT	4 HS
Point -3	4 LT	2 HS	5 HT	3.5 HS

the model predicts set-up in the north end and set-down in the south end of the two basins. Once the front passes and the wind directions shift to northerly, the water in the north end is set-down and the elevation in the south is set-up for both the Banana River and the IRL. Points-1 and -2 are located in the northern portion of the IRL, this wide shallow part of the domain experiences larger set-down, Figure 5(b), than that experienced at Point-3, Figure 5(a). There is a stronger signal at these two locations in the time series, Figures 4(a) and 4(b). The model validation results provide confidence that the grid and

modeling system are able to represent the wind-driven dominated flow that defines the circulation in the Northern IRL (Weaver *et al.*, 2016).

Ensemble Member Comparisons

The four simulations, Table 1, are compared (wind speed and direction, water surface elevation, and H_S) at each of the three analysis points, the starred locations in Figure 3. The maximum differences between the spatial simulation results and maximum differences between the temporal resolution results for both surface elevation and H_s at each point are provided in Table 4 for reference throughout this section.

During the period prior to the frontal passage (FROPA) on 6 March, wind directions are predominantly southerly at 5 m/s. While after its passage, the wind speed increases to over 10 m/s and the direction shifts to northerly.

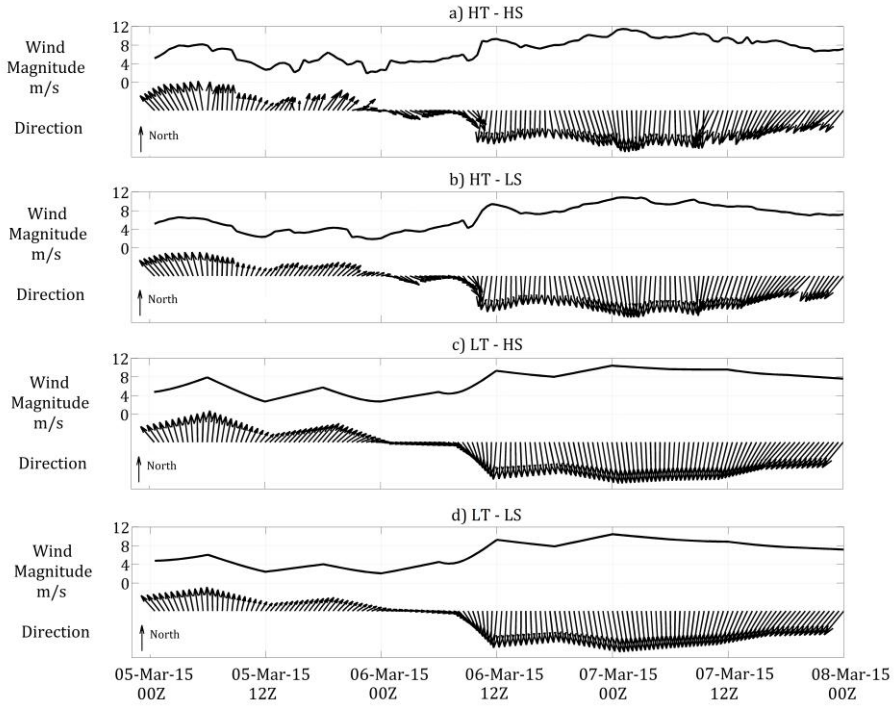

Figure 6: Time series of wind magnitude (m/s) and direction for the four ensembles in Table 1. From top to bottom: a) HT-HS, b) HT-LS, c) LT-HS, and d) LT-LS respectively at Point-1 in Box 1 (Fig. 3) for the 72 h period beginning 00 Z 5 March 2015.

Similar behavior was seen in the wind forcing throughout the domain. At each of the 3 analysis points, the wind magnitude and direction for the LT resolution ensemble members are noticeably smoother than that of the HT resolution. The hydrodynamic model linearly interpolates the input wind forcing

down to the model time step (1 s), this results in the LT (6 h) wind forcing exhibiting a smooth gradient in the wind magnitude and direction barbs between the 6 hourly input intervals, Figure 6. The HT and LT resolution wind forcing have the same values at the six hour intervals, which constrains the differences in the solutions. There are instances, most notably after the FROPA on 7 March, where the results of this constraint is evident in the surface elevation signal, Figure 7. The impact of LS resolution on the wind forcing is not as discernible from the wind vector plots.

There are more subtle differences between the LS and HS wind field, Figure 6. The HS resolution members can have up to 20-to-30% higher wind speeds than the LS (*e.g.,* Point-2 in Box-2). Differences in the wind magnitude at Points -1 and -3 are generally small, primarily due to the LS treating both Box 1 and 3 as water, Table 2.

Surface Elevation

Each of the four ensemble members predict the same general trend for water elevation though there is as much as a 10 cm difference in amplitude during the peak set-down between the HS and LS simulations at the northernmost analysis location, Point-1, Figure 7(a). Differences in the predicted surface elevation are greater than 30% near the peak set-down following the FROPA on 7 March, Figure 7. While this large difference seems contradictory to the small differences in the wind forcing at this point, the surface elevation is sensitive to the time integrated and spatially integrated wind field impacting the water body. The simplified steady-state momentum equation can be expressed as:

$$\rho(h+\eta)\left(g\,\frac{\partial \eta}{\partial x}\right) = \tau_{zx}(\eta) - \tau_{zx}(h) \qquad (1)$$

The left hand side term is the surface elevation gradient, balanced on the right hand side by the surface wind stress and bottom stress terms respectively. From the simplified balance it is easier to understand how changes in predicted water elevations are due in part to the upwind/downwind behavior of the input wind forcing and the hydrodynamic responses to that forcing.

Prior to the FROPA the wind magnitudes are lower and the wind direction is not as consistent as after the FROPA. There is a greater water elevation response after the front passes due both to the increase in wind magnitude, as well as the consistent direction and associated favorable fetch (*i.e.*, the post-frontal set-down is greater than the set-up associated with the southerly flow prior to its passage). After the front passes, and the north winds dominate the system, the water in the northern compartment decreases at all three points until the wind magnitudes begin to subside, Figure 7.

The surface elevation differences at Point-3, Figure 7(c), oscillate about zero and the amplitude is smaller than at the other two locations. As previously mentioned, Point-3 is at a location within the Banana River that does not experience a large range of water elevation changes, Figure 5(a). We calculate a maximum 5 cm difference between the surface elevation for the HS and LS ensemble members, Figure 7(c). The peak elevation change, 10 cm, occurs during the frontal event.

Significant Wave Height, H_S

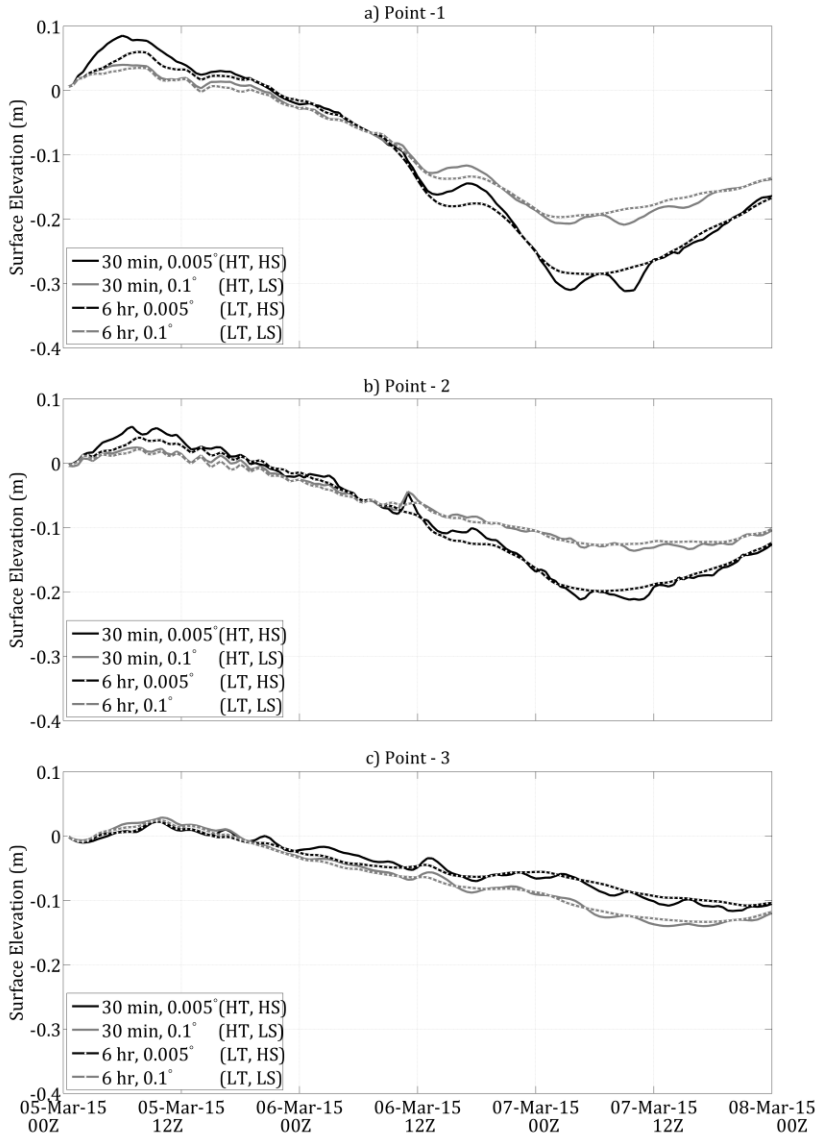

Figure 7: Time series of surface elevation (m) at (a) Point-1, (b) Point-2, and (c) Point-3 for the 72 h period beginning 00 Z 5 March 2015. The time series for each ensemble member, HT-HS, HT-LS, LT-HS, and LT-LS, are provided for comparison at each point. The LS simulation results are plotted in gray and the HS resolution results are plotted in black.

In the northern lagoon location, the significant wave heights show greater spread in association with lower wind magnitudes during the southerly pre-frontal period. As the front passes and the wind direction shifts and increases in magnitude, the water elevation sets down and wave heights grow with only small differences between the four members at Point-1, Figure 8(a). At this particular location, the water depth and fetch are constraining the wave growth (*i.e.,* mean water depth at Point-1 is -1.73 m NAVD88). Stations farther from the land boundary and in deeper water do not exhibit this same fetch and depth limited behavior.

Prior to the FROPA, 00 to 12 Z 6 March, as wind direction shifts from southerly to northerly, the fetch is reduced, and the wave heights gradually decay across the IRL until the post-frontal northerly flow increases both the fetch and magnitude of the wind.

At Point-1, the differences between the HS and LS ensemble member's wind magnitudes, Figure 6, are greatest prior to the FROPA. During this period, the winds are southerly while the upwind grid box (*i.e.*, Box 2 to the south) is characterized as land in the coarse resolution WRF, Table 2, which effectively reduces the fetch into Box 1. Differences are less for the northerly flow following the FROPA since both the HS and LS resolution members treat Box 1, the upstream box, as water.

In contrast to Point-1, Point-2 is in deeper water (-4 m NAVD88) and is located a greater distance from the northern land boundary (greater fetch), as a result, there is more variation in the post-frontal wave heights than at Point-1, Figures 8(a, b). In particular, the wave heights in the HS resolution simulations are consistently larger (by as much as 0.1 m) than the LS simulations throughout the duration of the event.

The spatial differences in the significant wave height early in the simulation, 00 Z 5 March to 00 Z 6 March, are higher for the HT cases than for the LT cases. Large differences in the H_S plots were seen at Point-1 only prior to the FROPA, Figure 8(a). During this same time period, the H_s differences between the two temporal resolution simulations are greatest.

The differences in H_S between the temporal ensemble members are smaller than the differences calculated between the spatial resolution members, Table 4. The maximum difference in predicted H_S, on the order of 5 cm, occurs in association with the peak post-frontal wind speeds and largest wave heights (near 30 cm) at Point-2 and -3, while at Point-1 the maximum difference occurs prior to the FROPA. The wave field is more sensitive than the surface elevation to the local wind field as the differences in H_S closely follow differences in the magnitude of the wind forcing (Ardhuin *et al.,* 2007; Booij *et al.*, 1999; Toba *et al.,* 1990). Our model results are in general agreement with the theory.

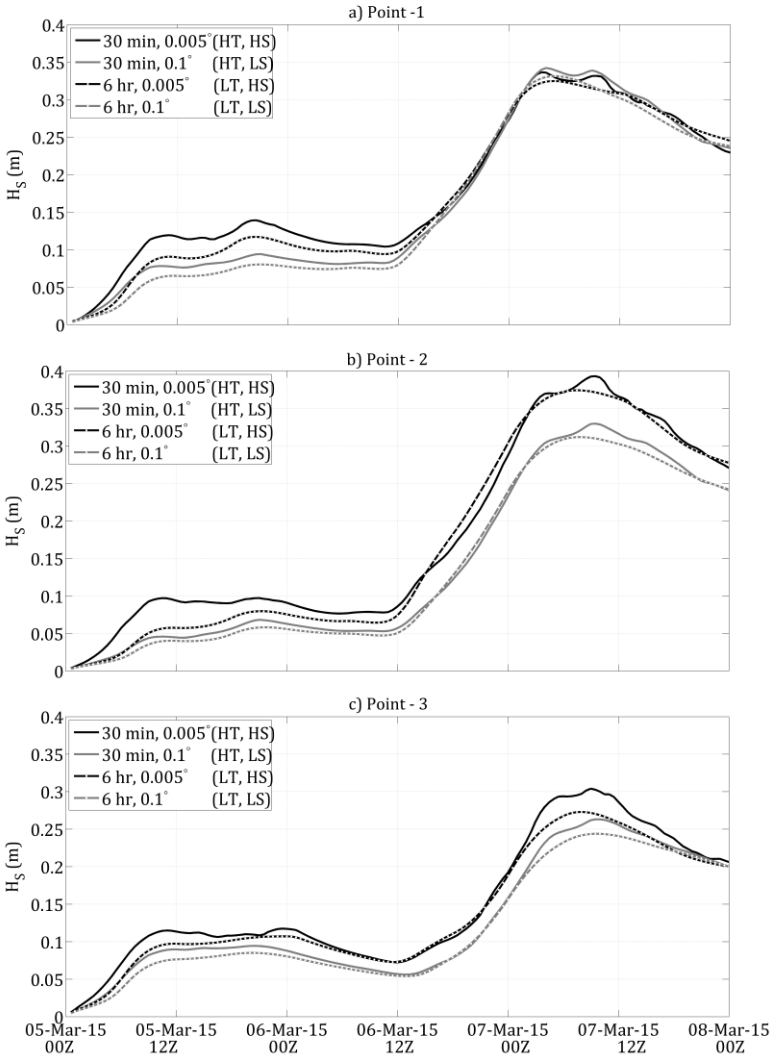

Figure 8: Time series of H_S (m) at (a) Point-1, (b) Point-2, and (c) Point-3 for the 72 h period beginning 00 Z 5 March 2015. The time series for each ensemble member, HT-HS, HT-LS, LT-HS, and LT-LS, are provided for comparison at each point. The LS simulation results are plotted in gray and the HS resolution results are plotted in black.

Analysis

Since the hydrodynamic model simulations are forced only by the meteorological input, we expect high values of the correlation of determination (R^2) between wind speed and both surface elevation and H_s for all simulations. R^2 values correlating wind speed and surface elevation ranged from 0.842 (Point-3, HT-HS) to 0.955 (Point-1, LT-LS), with the time lag for the HT simulations increasing from Point-1 to Point-2. Correlation between significant wind speeds and wave heights range from 0.86 (Point-2, HT-LS and LT-LS) to 0.936 (Point-1, HT-HS). The wave height correlates better with the local HS resolution wind forcing. Here, the lag in wave response also increases from Point-1 to -2 for the HT-HS and HT-LS simulations as the fetch for the northerly wind increases.

Discussion

In the northernmost analysis box, Box 1, both the HS and LS resolution ensemble members treat the lagoon as water. As a result, the changes in predicted water elevations must be due in part to the upwind and downwind behavior of the wind field within and outside the analysis box. Within grid Box 2, the LS resolution members treat the box as if it was land, while the HS forcing better resolves the land/water mask (*i.e.*, it has a combination of both land and water grid points). This has atmospheric flow-dependent implications for the hydrodynamic circulation in Box 1.

The low (high) spatial forcing simulations have land (water) upstream of Box 1 during a southerly wind. During the first 24 hours of the simulations, there is a significant fetch reduction for the wind forcing from the LS resolution members. As a result, the weaker wind magnitude pushes less water to the north (*i.e.*, from Box 2 into Box 1). In addition, the waves generated in Box 2 will be smaller for the LS resolution case than for the HS resolution case. For the HS resolution case, larger waves will be propagating from Box 2 into Box 1.

Conversely, for northerly winds, as water is pushed to the south in the HS resolution simulations, more water can flow from Box 1 into Box 2 than is the case for the LS resolution simulation. In the case of the HS simulation, stronger northerly winds in Box 2 than applied in the LS simulation generate a lower surface elevation gradient at the boundary between Box 1 and 2 allowing for more flow. Due to the reduced surface wind stress applied by the LS simulation in Box 2, there is more water flowing into Box 2 from Box 1 than there is leaving Box 2, and this difference results in a piling up of water and restriction of flow. The upstream wind field has an effect on the local circulation and set-up.

The spatial resolution of the meteorological forcing has not only a direct effect on the hydrodynamics from the local variations in the wind field, but also a basin-wide impact from the location of the land–water interface and subsequent land mask. The basin-wide impact of the land mask on the surface elevation prediction is due to the integral nature of the surface elevation in the momentum equation. The wave height prediction is impacted through the interaction between the wind speed and fetch.

These spatial resolution effects are not unique to the IRL, and should manifest in any coastal system where the length scales are smaller than the resolution of operational meteorological model being used to generate the forecast (*e.g.,* Virginia Coast Reserve, Albemarle-Pamlico Estuary System, Hawaii, northwest Mediterranean, lake simulations, Padre Island National Seashore/Baffin Bay, *etc.*). The meteorological forcing used to predict hydrodynamic and wave responses must accurately capture the land-water interface. Even in a large estuary system, if the purpose of the modeling effort is to generate a prediction of the response at the coast, including inundation, the spatial resolution of the forcing at the coast needs to be high enough to capture the local effects.

Conclusion

Based on the results from this study of a frontal passage in central Florida, it is determined that increases in the spatial resolution of the wind forcing yields a bigger impact on the circulation than increasing the temporal resolution. Varying the temporal resolution of the wind field forcing from 6 h to 30 min only marginally affects the results. The main driver for these differences in the case presented here is the land–water mask as seen by the meteorological model. In order for the forecast models to provide the best guidance, high spatial resolution wind forcing will be needed to capture the complex geography of the domain.

Acknowledgements

The work reported in this paper was supported with funds from NOAA and the National Weather Service Program Office (NWSPO), CSTAR Award #: NA14NWS4680014, "*An Ensemble-based Approach to Forecasting Surf, Set-Up and Surge in the Coastal Zone*". Meteorological data from WeatherFLow was used for meteorological model verification. Data from real-time gauges in place and managed by Saint John's River Water Management District (SJRWMD) was used for model calibration and verification, http://webapub.sjrwmd.com/agws10/hdswq/. U.S. Geological Survey (USGS) hydrologic station data from the Haulover Canal was used for model validation, http://waterdata.usgs.gov/usa/nwis/uv?site_no=02248380 .

Literature Cited

Alomar,M.,2012. Improving wave forecasting in variable wind conditions. The effect of resolution and growth rate for the Catalan coast (Ph.D.thesis). Universitat Politecnicade Catalunya.

Ardhuin, F., Herbers, T.H.C., Watts, K.P., van Vledder, G.P., Jensen, R. and Graber, H.C., 2007. Swell and slanting-fetch effects on wind wave growth.*Journal of Physical Oceanography*, *37*(4), pp.908-931.

Booij, N., Ris, R.C. and Holthuijsen, L.H., 1999. A third-generation wave model for coastal regions: 1. Model description and validation. *Journal of geophysical research: Oceans*, *104*(C4), pp.7649-7666.

Carvalho, D., Rocha, A., Gómez-Gesteira, M., Silva Santos, C. , 2014, WRF wind simulation and wind energy production estimates forced by different reanalyses: comparison with observed data for Portugal, *Appl Energy*, 117, pp. 116–126

Cheng, F.-Y., and D. W. Byun (2008), Application of high resolution land use and land cover data for atmospheric modeling in the Houston-Galveston metropolitan area: Part I. Meteorological simulation results, *Atmos. Environ.*, 42, 7795–7811, doi:10.1016/j.atmosenv.2008.04.055.

Cheng, R.T.; Casulli, V., and Gartner, J.W., 1993. Tidal, Residual, Intertidal Mudflat (TRIM) Model and its Applications to San Francisco Bar, California. *Estuarine, Coastal and Shelf Science,* 36(3), 235-280.

De Pondeca, M. S. F. V., and Coauthors, 2011: The Real-Time Mesoscale Analysis at NOAAs National Centers for Environmental Prediction: Current status and development. *Wea. Forecasting*, 26, 593–612, doi:10.1175/WAF-D-10-05037.1.

DiMego, G. J., Bosart, L. F., and Endersen, G. W., 1976: An Examination of the Frequency and Mean Conditions Surrounding Frontal Incursions into the Gulf of Mexico and Caribbean Sea. *Mon. Wea. Rev.,* 104, 709–718.

Dietrich, J.C., S. Tanaka, J.J. Westerink, C.N. Dawson, R.A. Luettich Jr., M. Zijlema, L.H. Holthuijsen, J.M. Smith, L.G. Westerink, H.J. Westerink, 2012, “Performance of the Unstructured-Mesh, SWAN+ADCIRC Model in Computing Hurricane Waves and Surge”, *Journal of Scientific Computing*, DOI: 10.1007/s10915-011-9555-6.

Dietrich, J. C., M. Zijlema, J. J. Westerink, L. H. Holthuijsen, C. Dawson, R. A. Luettich, R. Jensen, J. M. Smith, G. S. Stelling, and G. W. Stone, 2011, Modeling hurricane waves and storm surge using intergrally-coupled, scalable computations, *Coastal Engineering*, 58, 45–65

Environmental Modeling Center (EMC), 2003: The GFS Atmospheric Model. **NCEP Office Note 442**, Global Climate and Weather Modeling Branch, EMC, Camp Springs, Maryland.

Hope, M. E., J. J. Westerink, A. B. Kennedy, P. C. Kerr, J. C. Dietrich, C. Dawson, C. J. Bender, J. M. Smith, R. E. Jensen, M. Zijlema, L. H. Holthuijsen, R. A. Luettich Jr., M. D. Powell, V. J. Cardone, A. T. Cox, H. Pourtaheri, H. J. Roberts, J. H. Atkinson, S. Tanaka, H. J. Westerink, L. G. Westerink, 2013, Hindcast and validation of Hurricane Ike (2008) waves, forerunner, and storm surge, *J. Geophys. Res. Oceans*, 118, 4424–4460, doi:10.1002/jgrc.20314.

Horel, J.; Splitt, M.; Dunn, L.; Pechmann, J.; White, B.; Ciliberti, C.; Lazarus, S.; Slemmer, J.; Zaff, D., and Burks, J., 2002. Mesowest: Cooperative Mesonets in the Western United States. *Bull. Amer. Meteor. Soc.*, **83**, 211–225.

Hong, S.-Y., S. Y. Noh, and J. Dudhia, 2006: A new vertical diffusion package with an explicit treatment of entrainment processes.*Mon. Wea. Rev.*, 134, 2318–2341, doi:10.1175/MWR3199.1

Janjić, Z. I., T. L. Black, M. E. Pyle, H.-Y. Chuang, E. Rogers, and G. J. DiMego, 2005: The NCEP WRF-NMM core. Preprints, Joint WRF/MM5 User's Workshop, Boulder, CO, NCAR, 2.9.

Jimenez, P., J. Dudhia, J. Gonzalez-Rouco, J. Navarro, J. Moneavez, and E. Garcia-Bustamante, 2012: A revised scheme for the WRF surface layer formulation, *Monthly Wea. Review*, 140, 898-918.

Kjerfve, B., 1986. Comparative Oceanography of Coastal Lagoons. *Estuarine Variability,* 63-81.

Liu, J.T.; Zarillo, G.A., and Surak, C.R., 1997. The Influence of River Discharge on Hydrodynamics and Mixing in a Subtropical Lagoon. *Journal of Coastal Research*, 13(4), 1016-1034.

Luettich, R.A.; Cass, S.D.; Reynolds-Fleming, J.V.; Fulcher, C.W., and McNinch, J.E., 2002. Semi-diurnal seiching in a shallow, micro-tidal lagoonal estuary. *Continental Shelf Research,* 22(11-13), 1669-1681.

Luettich, R.A. and Westerink, J.J., 2004. *Formulation and Numerical Implementation of the 2D/3D ADCIRC Finite Element Model Version 44.XX*., R. Luettich, http://www.unc.edu/ims/adcirc/adcirc_theory_2004_12_08.pdf, 74p.

Mallard, M. S., C. G. Nolte, O. R. Bullock, T. L. Spero, and J. Gula, 2014: Using a coupled lake model with WRF for dynamical downscaling. *J. Geophys. Res. Atmos.*, 119, 7193–7208, doi:10.1002/2014JD021785.

Mied, R.P.; Schulz, W.J.; Handler, R.A.; Snow, C.M.; Fusina, R.A., and Porter, J.H., 2010. Remote and Local Forcing of a Coastal Lagoon: The Virginia Coast Reserve. *Continental Shelf Research,* 30(20), 2057-2066.

Muller H, Dumas F, Blanke B, Mariette V, 2007. High-resolution atmospheric forcing for regional oceanic model: the Iroise Sea. *Ocean Dyn* 57(4):375–400

Niedda, M. and Greppi, M., 2007. Tidal, seiche and wind dynamic in a small lagoon in the Mediterranean Sea. *Estuarine, Coastal and Shelf Science*, 74(1-2), 21-30.

Pawlowicz, R.; Beardsley, B., and Lentz, S., 2002. Classical tidal harmonic analysis including error estimates in MATLAB using T_TIDE, *Computers and Geosciences,* 28(8), 929-937.

Reynolds-Fleming, J.V. and Luettich, R.A., 2004. Wind-driven lateral variability in a partially mixed estuary. *Estuarine, Coastal, and Shelf Science*, 60(3), 395-407.

Saha, S, and Coauthors, 2014: The NCEP Climate Forecast System version 2. *J. Climate*, 27, 2185–2208, doi:10.1175/JCLI-D-12-00823.1

Santos-Alamillos, F.J., Pozo-Vázquez, D., Ruiz-Arias, J.A., Tovar-Pescador, J., 2015. Influence of land-use misrepresentation on the accuracy of WRF wind estimates: Evaluation of GLCC and CORINE land-use maps in southern Spain, *Atmospheric Research*, 157, pp. 17-28.

Sheng, Y.; Davis, J.; Sun, D.; Qiu, C.; Christian, D.; Park, K.; Kim, T., and Zhang, Y., 2002. Application of an Integrated Modeling System for Estuarine and Coastal Ecosystems to Indian River Lagoon, Florida. *Estuarine and Coastal Modeling*, 329-343.

Skamarock, W. C., and Coauthors, 2008: A description of the Advanced Research WRF version 3. NCAR Tech. Note NCAR/TN-475+STR, 125 pp.

Smith, N. P., 1990. Computer Simulation of Tide-Induced Residual Transport in a Coastal Lagoon. *Journal of Geophysical Research,* 95(C10), 18205-18211.

Smith, N.P., 2001. Seasonal-scale Transport Patterns in a Multi-inlet Coastal Lagoon. *Estuarine, Coastal and Shelf Science*, 52(1), 15-28

Stopa, J.E., K.F. Cheung, Y. Chen, 2011: Assessment of Wave Energy Resources in Hawaii. Renewable Energy, 36(2), February, 554-567.

Toba, Y., Iida, N., Kawamura, H., Ebuchi, N. and Jones, I.S., 1990. Wave dependence of sea-surface wind stress. *Journal of Physical Oceanography*, *20*(5), pp.705-721.

Vilibic, I. and Orlic, M., 1999. Surface Seiches and Internal Kelvin Waves Observed Off Zadar (East Adriatic). *Estuarine, Coastal and Shelf Science*, 48(1), 125-136.

Wackerly, D., Mendenhall, W. and Scheaffer, R., 2007. *Mathematical statistics with applications*. Nelson Education.

Weaver, R.J.; Johnson, J.E., and Ridler, M., 2016. Wind Driven Circulation in a Shallow Micro-Tidal Estuary: the Indian River Lagoon. *Journal of Coastal Research*, **doi:** http://dx.doi.org/10.2112/JCOASTRES-D-15-00046.1